frontiers | Frontiers in Mechanical Engineering

TYPE Original Research
PUBLISHED 09 December 2025
DOI 10.3389/fmech.2025.1707105

OPEN ACCESS

EDITED BY
Hamid Reza Karimi,
Polytechnic University of Milan, Italy

REVIEWED BY
Xingdong Sun,
Anhui Agricultural University, China
Zhiming Cheng,
Zhenjiang College, China

*CORRESPONDENCE
Jinqiu Shang,
shangjinqiu2022@163.com

RECEIVED 17 September 2025
REVISED 18 November 2025
ACCEPTED 24 November 2025
PUBLISHED 09 December 2025

CITATION
Shang J (2025) Automatic detection system for aircraft engine turbine blade faults based on improved PSO.
Front. Mech. Eng. 11:1707105.
doi: 10.3389/fmech.2025.1707105

Automatic detection system for aircraft engine turbine blade faults based on improved PSO

Jinqiu Shang*

Aviation Maintenance Institute, Jiangsu Aviation Technical College, Zhenjiang, China

Introduction: With the increase of human travel, aviation activities become more frequent, and flight safety gains more attention. Faults in aircraft engine turbine blades seriously threaten flight safety, while traditional detection methods face problems of low accuracy and efficiency, making them insufficient for complex operating conditions.
Methods: This study raises an automatic detection system for aircraft engine turbine blade faults based on improved Particle Swarm Optimization. The system integrates the advantages of Grey Wolf Optimization, Genetic Algorithm, and Particle Swarm Optimization, and builds an adaptive feature selection mechanism. It combines Relevance Vector Machine classification to train the fault detection model, completing automatic detection of turbine blade faults. Experimental results show that after 80 iterations, the system error decreases to 0.08×10^{-3}, and the fault prediction accuracy reaches 98.33% improving by 9.16% compared with the reference system. With increased data volume, the prediction accuracy and response time reach 0.99 and 0.5 s respectively, demonstrating significantly better performance than the comparison system.
Results and Discussion: These results indicate that the proposed system achieves efficient and accurate detection of turbine blade faults. It provides an intelligent detection solution for aircraft engine maintenance, improves fault identification accuracy and efficiency, reduces flight safety risks, and promotes the development of intelligent diagnosis technology for aviation equipment, showing engineering application and promotion value.

KEYWORDS

PSO, GA, GWO, RVM, bayesian optimization

1 Background

Aircraft engines, as the core power units of airplanes, rely on the reliable operation of turbine blades for flight safety (Bhandari et al., 2023a). Under complex aviation operating conditions, turbine blades are easily affected by high temperature, high pressure, and strong vibration, leading to cracks, wear, and other faults. Failure to detect these faults accurately and timely may cause serious safety accidents (Bhandari et al., 2023b). Therefore, developing an efficient and accurate automatic detection system for turbine blade faults becomes a key demand in the aviation power field. Currently, relevant research explores turbine blade fault detection from multiple perspectives. Machine learning algorithms such as Extreme Gradient Boosting and two-dimensional Convolutional Neural Networks are applied for fault identification, improving detection efficiency to some extent. Nevertheless, under the highly dynamic and complex operating conditions of aircraft engines, these methods continued to exhibit constraints in terms of accuracy and robustness (Wang et al., 2025; Kiliç and arslan, 2023). Traditional single algorithms struggle to adapt to the complex

features of turbine blade faults. Models show weak generalization for multi-condition and small-sample data, failing to meet the strict requirements of fault detection in aviation (Purohit and Dave, 2023; Bhandari et al., 2024). Therefore, this study raises an improved Particle Swarm Optimization (PSO) algorithm by integrating the advantages of Grey Wolf Optimization (GWO) and Genetic Algorithm (GA), building an adaptive optimization framework. The improved PSO retains the global search capability of PSO while leveraging the group intelligence of GWO and the genetic mechanism of GA to enhance the ability to escape local optima and improve convergence efficiency. Combined with the improved Relevance Vector Machine (RVM), the system accurately extracts turbine blade fault features and completes fault classification. In this way, the study constructs an automatic detection system for aircraft engine turbine blade faults by integrating improved PSO and improved RVM, achieving efficient and accurate fault identification under complex operating conditions. Its innovation lies in the collaborative optimization of algorithm fusion and feature extraction, overcoming the limitations of traditional methods. The system is expected to provide intelligent and reliable detection solutions for aircraft engine maintenance, contributing to the reliability of aviation power systems.

2 Literature review

PSO is a swarm intelligence optimization technique that draws inspiration from the foraging patterns observed in bird flocks. It has shown strong optimization ability in engineering optimization, signal processing, machine learning, and other fields. Many scholars have conducted research on it. Demir and Sahin addressed the problem of catastrophic damage caused by lateral expansion due to liquefaction on lifelines and buildings. They proposed a powerful machine learning algorithm and used PSO to optimize the hyperparameters of the gradient boosting model, improving its prediction performance (Demir and Sahin, 2023). In response to the problem that heart disease has become the number one cause of death worldwide, scholars such as El-Shafiey et al. developed a hybrid optimization method based on random forest, genetic algorithm and particle swarm optimization. Selecting the optimal features that contribute to higher predictive accuracy enables more reliable detection of heart disease (El-Shafiey et al., 2022). In response to the problem that machine learning technology cannot accurately predict civil structures with low damage, Cuong-Le and his team proposed a damage identification method that combines particle swarm optimization and support vector machine. The effective search capability of particle swarm can eliminate redundant input parameters, and the support vector machine technology can effectively classify the damage location (Cuong-Le et al., 2022). Rao et al. focused on managing and controlling credit risk of personal auto loans in P2P network lending. They proposed an improved feature selection method to choose evaluation indicators for credit risk and combined PSO with gradient boosting to assess loan credit risk (Rao et al., 2023). Li and Fan highlighted the critical role of PSO in planning urban green space landscapes. They introduced a PSO-backpropagation neural network that integrated landscape ecology concepts with the strong memory and learning capabilities of PSO-BP, allowing for a more thorough evaluation and prediction of urban green space planning strategies (Li and Fan, 2022).

Turbine blades are core components in aircraft engines, gas turbines, and other power units that endure extreme operating conditions, directly determining engine performance. Accurate fault detection of turbine blades can greatly reduce safety accidents. Many scholars have conducted research in this area. Wang et al. addressed the problem of large parameter quantity and computational complexity in deep learning models for inner diameter inspection. They proposed a lightweight blade damage detection model that used an inverse residual structure to lighten the backbone network of the SSD model and optimized the scale and number of anchor boxes with a clustering algorithm, reducing model parameters and computational complexity (Wang et al., 2024). Amjad et al. proposed a multi-indicator evaluation method to assess fault detection capability, combining statistical validity with adaptability (Amjad et al., 2025). Xu et al. developed a digital twin-assisted, multi-view reconstruction graph network with enhanced domain adaptation for diagnosing faults in aircraft engine gas path systems (Xu et al., 2024). Ogaili et al. recognized that effective structural monitoring can maximize wind turbine efficiency. They proposed a wind turbine blade fault detection model combining Discrete Wavelet Transform and Fast Fourier Transform. Through multi-resolution analysis of vibration signals, they identified frequency sub-bands containing local fault information (Ogaili et al., 2024). Liu et al. focused on the high-precision manufacturing requirements of turbine blades for wind engines. They proposed a feature-based non-contact quality prediction and parameter optimization framework for high-precision multi-material processing, using a local gradient search improved preheating optimization algorithm to optimize key initial machining features and improve final production quality (Liu et al., 2023).

In summary, existing research has achieved some results in turbine blade fault detection, but traditional machine learning algorithms have limited ability to capture complex fault features. The feature selection methods used are inefficient in removing high-dimensional redundant features, affecting system convergence speed and detection accuracy. Therefore, this study raises a hybrid algorithm integrating PSO, GA, and GWO, combined with a classification system using RVM, Bayesian Optimization (BO), and Simulated Annealing (SA), to complete automatic detection of aircraft engine turbine blade faults. The system achieves both recognition accuracy and speed, and it is expected to effectively reduce flight safety risks and safeguard aviation power systems. The innovation of this study lies in the proposed GWO-GA-PSO hybrid optimization algorithm, which applies the hunting-style local search of GWO, the genetic crossover mutation diversity maintenance of GA, and the global speed advantages of PSO to high-dimensional vibration data of aircraft engines, effectively improving fault identification capabilities. The design of the ISA-RVM-BO lightweight classification framework solves the problems of model overfitting and time-consuming parameter adjustment under small sample sizes. The contribution of this study is that the GWO-GA-PSO hybrid algorithm and the ISA-RVM-BO classification framework provide a new algorithm fusion approach and adaptive optimization paradigm for complex industrial equipment fault detection. The constructed GGP-IRB achieves

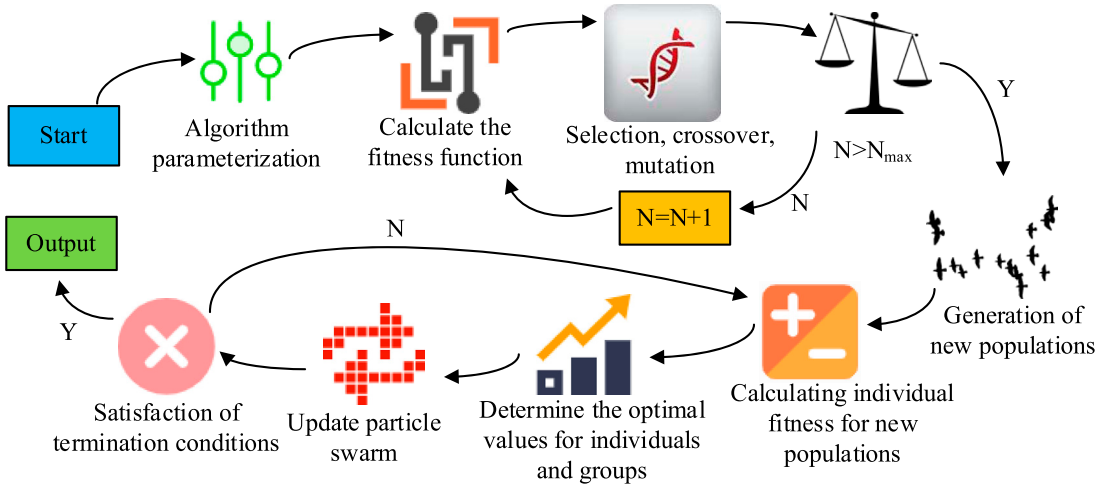

FIGURE 1
Schematic diagram of the GA-PSO operation process (Icon source from: https://www.iconfont.cn).

efficient and accurate fault detection, solving the problems of low accuracy and insufficient efficiency of traditional methods. This research promotes the engineering application and development of intelligent diagnosis technology for aviation equipment and has practical promotion value.

3 Model construction for aircraft engine turbine blade fault detection

3.1 Improved PSO algorithm design with GWO and GA

PSO is an efficient swarm intelligence optimization algorithm and shows unique advantages in turbine blade fault detection for aircraft engines. The fundamental principle of PSO is to emulate the cooperative foraging behavior of birds, enabling rapid exploration of the solution space to identify the optimal solution. Therefore, this study uses PSO to optimize feature extraction for turbine blade fault detection. However, basic PSO converges quickly through information sharing among particles, but it tends to fall into local optima in the later stages due to insufficient population diversity. To address this problem, GA is introduced to optimize PSO. The selection, crossover, and mutation operations of GA maintain population diversity and prevent premature convergence. Thus, GA-PSO enhances global search ability, accelerates convergence, and reduces the chance of falling into local optima (Khodsuz and Mashayekhi, 2023). Its operation is shown in Figure 1.

As shown in Figure 1, the hybrid algorithm first performs initialization and parameter setting. Parameter setting directly affects the search efficiency and accuracy of the algorithm, so it needs to meet the requirements of turbine blade fault detection. Then, fitness is calculated. The selection, crossover, and mutation operations of GA expand the search range and explore potential better solutions. After that, particles are updated based on their historical best position and the global best position. Finally, the termination condition is checked. If the condition is not met, the iteration continues. If the condition is met, the optimal model parameters are output. The selection operation of GA is expressed in Equation 1.

$$P_i = \frac{f(x_i)}{\sum_{j=1}^{N} f(x_j)} \tag{1}$$

In Equation 1, N is the population size, $f(x_i)$ is the fitness value of individual i, and P_i is the selection probability. The crossover operation is expressed in Equation 2.

$$\begin{cases} y^1 = (x_1^1, \cdots, x_k^1, x_{k+1}^2, \cdots, x_n^2) \\ y^2 = (x_1^2, \cdots, x_k^2, x_{k+1}^1, \cdots, x_n^1) \end{cases} \tag{2}$$

In Equation 2, $x^1 = (x_1^1, x_2^1, \cdots, x_n^1)$ and $x^2 = (x_1^2, x_2^2, \cdots, x_n^2)$ are two parent chromosomes, k is a random crossover point, and y^1 and y^2 are offspring chromosomes. Chromosome, $x = (x_1, x_2, \cdots, x_n)$ the mutation operation of GA, is expressed in Equation 3.

$$x_i' = \begin{cases} 1 - x_i, P_m \\ x_i, 1 - P_m \end{cases} \tag{3}$$

In Equation 3, P_m is the mutation probability. The velocity update of PSO is shown in Equation 4.

$$\begin{aligned} v_{id}(t+1) = \omega v_{id}(t) + c_1 r_{1d}(t)\left(p_{id}(t) - x_{id}(t)\right) \\ + c_2 r_{2d}(t)\left(g_d(t) - x_{id}(t)\right) \end{aligned} \tag{4}$$

In Equation 4, ω is the inertia weight used to balance global and local search abilities, c_1 and c_2 are learning factors, $r_{1d}(t)$ and $r_{2d}(t)$ are random numbers within [0, 1], D represents the dimension, and t represents the iteration number. GA-PSO enhances global search and improves the ability to escape local optima, but it still suffers from slow convergence and parameter tuning difficulties in the later stages. Therefore, this study introduces GWO to enhance local optimization and accelerate convergence. The flowchart of GWO is shown in Figure 2.

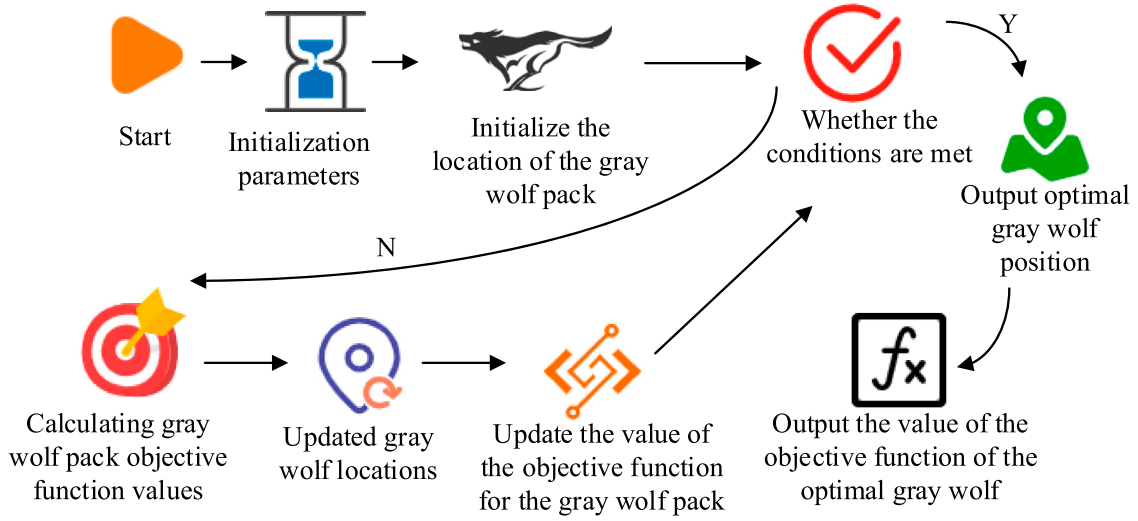

FIGURE 2
GWO operation flow chart (Icon source from: https://www.iconfont.cn).

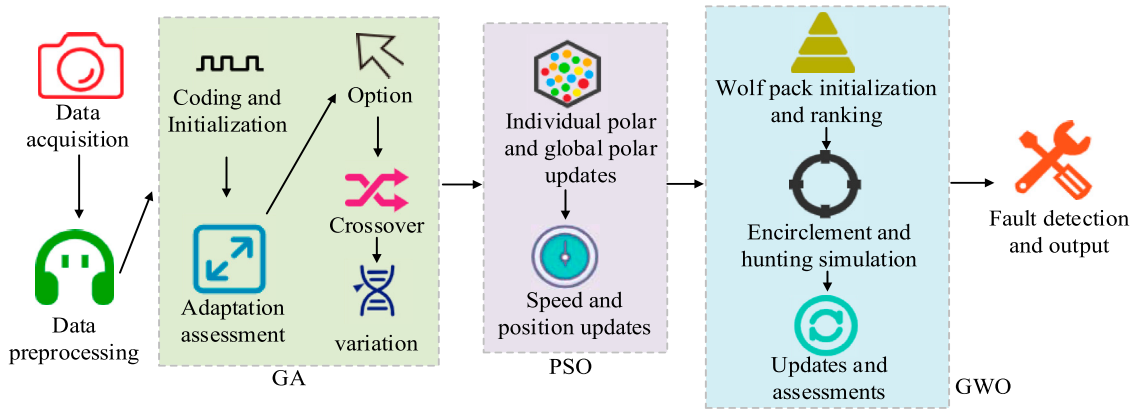

FIGURE 3
Operation flow chart of GWO-GA-PSO (Icon source from: https://www.iconfont.cn).

As shown in Figure 2, the algorithm first initializes parameters, including population size, maximum iterations, and search space dimensions. Then, the wolf pack positions are initialized by randomly generating the initial positions of grey wolves. The preset objective function evaluates each position to calculate fitness. After that, the positions of grey wolves are updated, and the objective function values are recalculated to evaluate the updated positions. Finally, the termination condition is checked. If it is met, the result is output. The convergence factor a in GWO is expressed in Equation 5.

$$a = 2 - t \times \frac{2}{T_{max}} \tag{5}$$

In Equation 5, t is the current iteration number, T_{max} is the maximum iteration number, and a takes values within the range of $[0, 2]$. The coefficient vector is shown in Equation 6.

$$\begin{cases} A = 2a \cdot r_1 - a \\ C = 2 \cdot r_2 \end{cases} \tag{6}$$

In Equation 6, A determines the direction and step size of individual position update, and C simulates the random movement of the prey. r_1 and r_2 are random vectors within the range of $[0, 1]$. Grey wolves gradually encircle the prey during hunting, expressed mathematically in Equation 7.

$$\begin{cases} D = \left| C \cdot X_p(r) - X(t) \right| \\ X(t+1) = X_p(t) - A \cdot D \end{cases} \tag{7}$$

In Equation 7, t is the current iteration number, $X(t)$ is the current position of the grey wolf, and $X_p(t)$ is the position of the prey. Finally, the workflow of the hybrid algorithm GWO-GA-PSO, optimized by GWO, is shown in Figure 3.

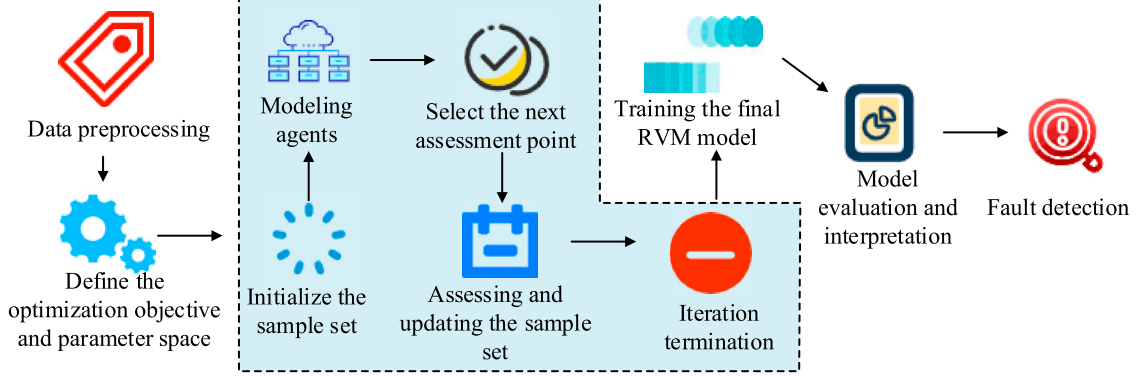

FIGURE 4
RVM-BO system structure diagram (Icon source from: https://www.iconfont.cn).

As shown in Figure 3, the algorithm consists of five parts. First is data acquisition and preprocessing. The second is the GA module. In GA, encoding and initialization are performed, then fitness is evaluated, and finally selection, crossover, and mutation are completed. The next part is PSO. In PSO, individual best and global best are updated first, then velocity and position are updated. The fourth part is deep optimization using GWO. In GWO, the wolf pack is initialized and ranked, then encircling and hunting simulation is performed to update wolf pack positions, and fitness values are recalculated to evaluate the effect. The last part is fault detection and output, completing the turbine blade fault judgment.

3.2 Automatic detection system for turbine blade faults combining improved PSO and RVM

Although the GWO-GA-PSO effectively extracts fault feature signals of aero-engine turbine blades, it does not perform well in fault diagnosis and classification. It also fails to explain and quantify fault diagnosis. Therefore, this study uses the RVM-BO system to achieve automatic fault detection of turbine blades. The high sparsity of the system supports efficient feature learning and lightweight performance. The Bayesian framework of RVM regularizes the model with prior knowledge, reducing the dependence on large amounts of labeled data. The sample efficiency of BO reduces the demand for data during system tuning, addressing the problem of scarce turbine blade fault samples (An et al., 2025). The structure of the RVM-BO system is shown in Figure 4.

As shown in Figure 4, the system first preprocesses the data, then defines the optimization objective and parameter space. BO then guides the parameter search through the surrogate model and acquisition function to obtain the optimal parameters. These optimal parameters train the final RVM system, and the system then performs performance evaluation and fault prediction. The prediction function of RVM is achieved through a linear combination of kernel functions, as shown in Equation 8.

$$f(x) = \sum_{i=1}^{N} \omega_i K(x, x_i) + b \tag{8}$$

In Equation 8, ω_i is the weight parameter, b is the bias term, x_i is the training sample, and $K(x, x_i)$ is the kernel function. RVM achieves sparsity through a Gaussian prior, and its weight prior is shown in Equation 9 (Dong et al., 2023).

$$p(\omega_i|a_i) = N(\omega_i \mid 0, a_i^{-1}) = \sqrt{\frac{a_i}{2\pi}} exp\left(-\frac{a_i \omega_i^2}{2}\right) \tag{9}$$

In Equation 9, $a_i > 0$ is the precision parameter, and each weight ω_i independently follows a zero-mean Gaussian distribution. BO models the objective function $f(x)$ using a Gaussian process, as shown in Equation 10.

$$f(x) \sim GP(m(x), k(x, x')) \tag{10}$$

In Equation 10, $m(x) = \mathrm{E}[f(x)]$ is the mean function, and $k(x, x')$ is the kernel function that describes the correlation between samples. The acquisition function of BO selects the next evaluation point and balances exploration and exploitation. The equation for Expected Improvement (EI) is shown in Equation 11.

$$\begin{aligned} EI(x) &= \mathrm{E}[\max\backslash(f(x) - f^*, 0] \\ &= \begin{cases} (\mu(x) - f^*)\Phi(z) + \sigma(x)\phi(z)\sigma(x) > 0 \\ 0 \quad \sigma(x) = 0 \end{cases} \end{aligned} \tag{11}$$

In Equation 11, f^* is the current optimal value, Φ and ϕ are the CDF and PDF of the standard normal distribution, respectively. Although RVM-BO shows significant advantages in fault monitoring, it has key limitations. For example, the hyperparameters of RVM are sensitive and easily fall into local optima, and the optimization performance of BO depends on initial samples (Khatti and Grover, 2025). To address this problem, this study uses SA to optimize the hyperparameters of RVM and the acquisition function of BO, which effectively improves small-sample adaptability and computational efficiency. However, the temperature parameters of SA also require tuning. Therefore, an Improved Simulated Annealing (ISA) is used to dynamically adjust the cooling and iteration strategy, reduce parameter tuning complexity, and allow early convergence when no improvement occurs after continuous iterations. The workflow of ISA is shown in Figure 5.

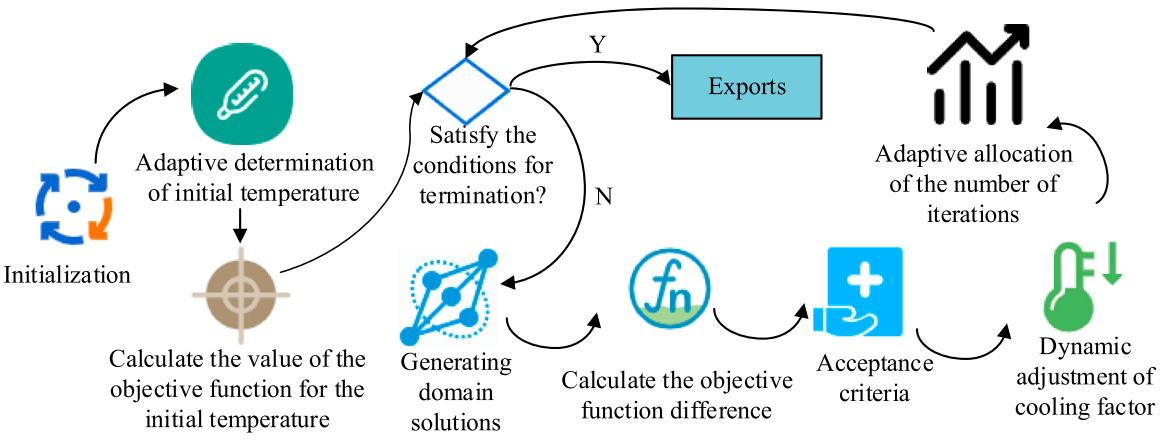

FIGURE 5
ISA operation flow chart (Icon source from: https://www.iconfont.cn).

As shown in Figure 5, the core idea of ISA is to dynamically adjust the temperature decay rate and iteration count based on the current search state. ISA first initializes and adaptively determines the initial temperature. It then calculates the objective function value at the current temperature and checks whether it meets the termination condition. If not, it generates a neighboring solution. The neighboring solution is evaluated by the objective function, and if it satisfies the acceptance criterion, it is adjusted using an adaptive temperature coefficient. After iteration optimization, it outputs the parameter tuning result. ISA calculates a reasonable initial temperature T_0 based on the difference in the objective function of initial solutions. The equation for the average difference of the objective function is shown in Equation 12.

$$\Delta f_{avg} = \frac{1}{N^2}\sum_{i,j}\left|f(x_i) - f\left(x_j\right)\right| \tag{12}$$

In Equation 12, $f(x_i)$ represents the calculated objective function value, and N is the number of initial solutions. SA simulates the process of high-temperature random search and low-temperature directional convergence in physical annealing. By introducing the Metropolis criterion, SA enhances the global search ability. The Metropolis criterion allows a certain probability of accepting solutions with worse objective values, as shown in Equation 13.

$$P = \begin{cases} 1 & \triangle f < 0 \\ exp\left(-\frac{\triangle f}{T}\right) & \triangle f \geq 0 \end{cases} \tag{13}$$

In Equation 13, P represents the acceptance probability of a new solution, $\triangle f$ is the objective value difference between the new and current solutions, and T is the current temperature. To simulate the gradual decrease of temperature during physical annealing, SA reduces the temperature according to a certain rule, as shown in Equation 14.

$$T_{k+1} = a \times T_k \tag{14}$$

In Equation 14, T_k is the temperature at the k -th iteration, T_{k+1} is the temperature at the $k+1$-th iteration, and a is the cooling coefficient, which is a constant between 0 and 1. Finally, based on the GWO-GA-PSO and ISA-RVM-BO, the aero-engine turbine blade fault automatic detection system is named GGP-IRB, and its overall workflow is shown in Figure 6.

In Figure 6, the system consists of a feature optimization module and a fault detection module. The system first collects and preprocesses the data, followed by feature optimization based on GWO-GA-PSO to select the optimal subset. GA performs selection, crossover, and mutation to optimize the population. PSO updates particle velocity and position to achieve global search, and GWO performs deep optimization. The next part constructs the fault detection system based on ISA-RVM-BO. ISA optimizes the key parameters of RVM-BO, and then RVM-BO performs fault classification. The fourth step is system training and fault detection. The trained classification system performs fault category detection. If the result does not meet expectations, it returns to the corresponding step for optimization until the system performance reaches the target. The proposed system uses GA population evolution, PSO global search, and GWO fine hunting to select the most sensitive feature subset for faults such as blade cracks and wear from the high-dimensional feature space, which can effectively improve the quality of input data and provide high discrimination input for subsequent classifiers. The selected optimal feature subset is directly used as input for the ISA-RVM-BO module. At the same time, the ISA algorithm was used to dynamically optimize the hyperparameters of the RVM-BO classifier and the Bayesian optimized acquisition function, effectively solving the problems of RVM hyperparameter sensitivity and BO initial sample dependence, thereby achieving efficient, accurate, and robust detection of turbine blade faults in aircraft engines.

4 Performance analysis of turbine blade fault automatic detection system

4.1 Superiority verification of GWO-GA-PSO algorithm

To verify the superiority of the GWO-GA-PSO fault identification algorithm, it was compared with Graph

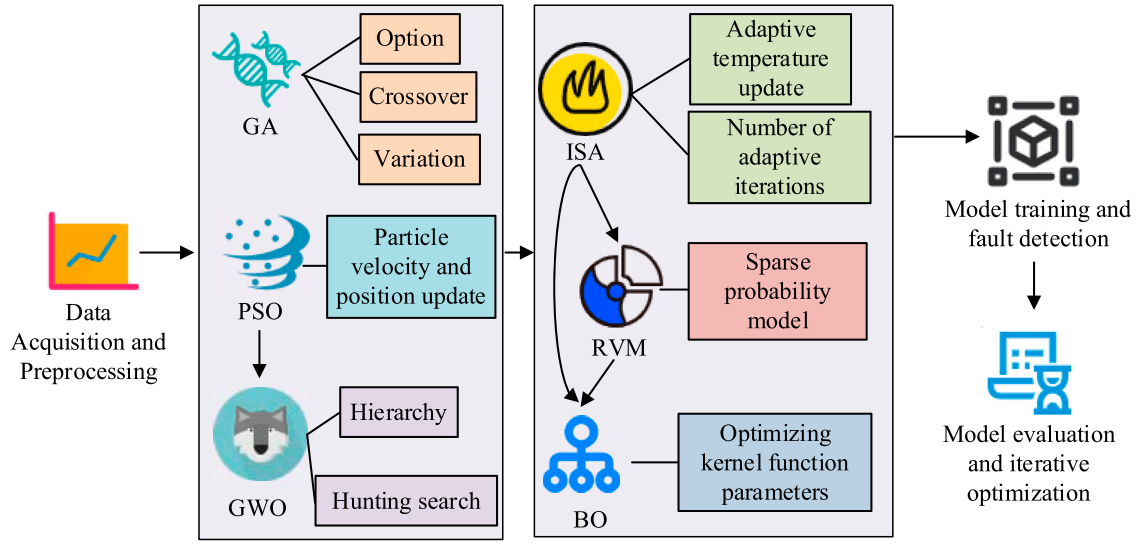

FIGURE 6
Overall flow chart of GGP-IRB (Icon source from: https://www.iconfont.cn).

Convolutional Network (GCN), Transformer, Improved Firefly Algorithm-eXtreme Gradient Boosting (IFA-XGBoost), Self Attention-Two-Dimensional Convolutional Neural Network (SA-2DCNN), and Relevance Vector Machine-Adaptive Neuro-Fuzzy Inference System (RVM-ANFIS). The experimental system ran on Windows 10 with an Intel Core i9-10900K CPU, RTX 4090 GPU, 512 GB memory, and Python 3.8. The experimental parameter settings of each algorithm are shown in the Table 1.

The datasets used were the Commercial Modular Aero-Propulsion System Simulation (C-MAPSS) and the AeBAD aero-engine blade anomaly detection dataset, both covering a wide range of operating conditions suitable for blade fault detection. A unified data processing procedure was used, with the k-nearest neighbor algorithm used to fill missing values. Z-score normalization was performed on all features to eliminate dimensionality differences. The isolation forest algorithm was used to detect and remove extreme outliers. Because time series data was used, a sliding window method was used to partition the samples, with a window size of 200 samples and a step size of 50 samples. Each window was treated as an independent sample, ultimately forming an input format suitable for fault detection. The C-MAPSS dataset consists of four subsets, FD001-FD004. This study selected FD001 and FD003. Data with a RUL of ≤30 cycles were labeled as faulty, and data with a RUL of >30 cycles were labeled as normal. A total of 12,000 valid samples were extracted, with 7,200 in the normal class and 4,800 in the fault class. These samples were divided into training, validation, and test sets in a 7:1:2 ratio, and 5-fold cross-validation was used to verify generalization performance. The AeBAD dataset includes normal, cracked, and worn blades. The two merged classes were classified as faulty, with the first class retained as normal. A total of 8,000 valid samples were extracted, including 3,200 normal and 4,800 faulty. The partitioning method and cross-validation rules used in C-MAPSS were identical to those used in the previous experiment to ensure a fair comparison. The key fault-sensitive features are mainly screened out through algorithms. In the diagnosis of aircraft engine turbine blade faults, the fault-sensitive features mainly include vibration signal features, temperature field features, and pressure pulsation features. The vibration signal features reflect the overall energy level and impact components of the blade vibration. Faulty blades often have increased vibration energy and abnormal peaks due to cracks or wear. The temperature field features reflect the thermal operating state of the blade and the effectiveness of the cooling system. Normal blades are cooled and regulated with uniform temperature distribution. When wear or cracks occur, local heat dissipation is hindered, which will lead to an increase in the temperature difference between different areas of the blade and obvious abnormalities in the temperature gradient distribution. The pressure pulsation features reflect the stability of the engine flow field and the aerodynamic performance of the blade. Faulty blades will destroy the flow field balance due to structural or shape changes, causing the pressure pulsation frequency to shift and the pulsation amplitude to increase significantly, which directly reflects the interference of blade failures on airflow movement. To evaluate the classification ability of GWO-GA-PSO, we used these two datasets to test it against three other algorithms. Statistical analysis was performed using an independent sample t-test, with a significance level of 0.05 and $p < 0.05$ indicating statistically significant differences. The test results are shown in Table 2.

As shown in Table 2, on the C-MAPSS dataset, the GWO-GA-PSO algorithm achieved precision, recall, and F1-score of 98.00% ± 0.32%, 98.49% ± 0.28%, and 98.24% ± 0.25%, respectively. Its precision was 3.75%, 3.00%, and 6.75% higher than those of IFA-XGBoost, SA-2DCNN, and RVM-ANFIS, respectively. Its recall was 6.09%, 4.20%, and 5.61% higher than those of the other three algorithms, respectively. Its F1-score was 4.92%, 3.60%, and 6.18% higher than those of the other three algorithms, respectively. The differences in all metrics between the compared algorithms and GWO-GA-PSO were statistically significant ($p < 0.05$). This indicates that the algorithm, through its hybrid feature

TABLE 1 Experimental parameters.

Algorithm	Parameters	Parameter value/Setting rules
GWO-GA-PSO	PSO population size	50
	Maximum number of iterations	500
	PSO inertia weight	(0.4, 0.9)
	Learning factor	$c_1 = c_2 = 2$
	GA crossover rate	0.8
	GA mutation rate	0.05
	GA selection strategy	Roulette method
ISA-RVM-BO	ISA initial temperature	100 °C
	ISA cooling coefficient	0.95
	ISA Markov chain length	100
	Early convergence threshold	The number of iterations is 50
	RVM kernel function	Radial basis kernel
	Bandwidth	0.1–10.0
	BO agent model	Gaussian process
	Get function	EI
	Number of iterations	50
IFA-XGBoost	IFA population size	40
	IFA attractiveness factor	0.5
	XGBoost tree depth	6
	Learning rate	0.1
	Number of iterations	100
SA-2DCNN	Convolution kernel size	3 × 3
	Number of convolution layers	3
	Number of self-attention heads	4
	Batch size	64
	Learning rate	0.0001
	Number of iterations	200
RVM-ANFIS	RVM kernel function	Radial basis kernel
	Number of ANFIS fuzzy rules	25
	Training epochs	150
GCN	Number of convolutional layers	2
	Activation function	ReLU
	Batch size	64
	Learning rate	0.001
	Number of iterations	200
	Regularization coefficient	0.0001

(Continued on following page)

TABLE 1 (*Continued*) Experimental parameters.

Algorithm	Parameters	Parameter value/Setting rules
Transformer	Number of attention heads	4
	Number of encoder layers	2
	Temporal attention window size	128 sampling points
	Batch size	64
	Learning rate	0.0001
	Number of iterations	250

TABLE 2 Comparison of classification capabilities of several models.

Dataset	Algorithm	Accuracy (%)	*p*-value compared with GWO-GA-PSO	Recall rate (%)	*p*-value compared with GWO-GA-PSO	F1-score (%)	*p*-value compared with GWO-GA-PSO
C-MAPSS	GWO-GA-PSO	98.00 ± 0.32	<0.05	98.49 ± 0.28	<0.05	98.24 ± 0.25	<0.05
	IFA-XGBoost	94.25 ± 0.67	<0.05	92.40 ± 0.81	<0.05	93.32 ± 0.72	<0.05
	SA-2DCNN	95.00 ± 0.53	<0.05	94.29 ± 0.64	<0.05	94.64 ± 0.58	<0.05
	RVM-ANFIS	91.25 ± 0.94	<0.05	92.88 ± 0.79	<0.05	92.06 ± 0.85	<0.05
	GCN	96.15 ± 0.48	<0.05	96.35 ± 0.45	<0.05	97.24 ± 0.31	<0.05
	Transformer	96.72 ± 0.41	<0.05	97.49 ± 0.35	<0.05	91.07 ± 0.87	<0.05
AeBAD	GWO-GA-PSO	97.00 ± 0.41	<0.05	97.49 ± 0.35	<0.05	97.24 ± 0.31	<0.05
	IFA-XGBoost	90.50 ± 0.82	<0.05	91.65 ± 0.93	<0.05	91.07 ± 0.87	<0.05
	SA-2DCNN	93.75 ± 0.61	<0.05	92.36 ± 0.75	<0.05	93.05 ± 0.68	<0.05
	RVM-ANFIS	88.50 ± 1.02	<0.05	89.62 ± 0.98	<0.05	89.06 ± 0.95	<0.05
	GCN	94.58 ± 0.55	<0.05	94.12 ± 0.58	<0.05	94.35 ± 0.56	<0.05
	Transformer	95.23 ± 0.47	<0.05	94.86 ± 0.50	<0.05	95.04 ± 0.48	<0.05

selection capability, can effectively capture fault-sensitive features in high-dimensional simulation data, achieving extremely low missed detection and false detection rates. On the AeBAD dataset, GWO-GA-PSO achieved precision, recall, and F1-score of 97.00% ± 0.41%, 97.49% ± 0.35%, and 97.24% ± 0.31%, respectively, significantly higher than the other algorithms. There was a significant difference between GWO-GA-PSO and the comparison algorithms ($p < 0.05$). Overall, GWO-GA-PSO achieved the best overall performance. To further demonstrate its superiority, the four algorithms were tested on C-MAPSS to observe their accuracy and loss rate evolution. The curves are shown in Figure 7.

As shown in Figure 7a, GWO-GA-PSO stabilized after 150 iterations, with the final accuracy reaching 0.95. SA-2DCNN stabilized after 250 iterations with an accuracy of 0.90, while IFA-XGBoost and RVM-ANFIS stabilized after 300 and 350 iterations, respectively, and neither reached 90% accuracy. As shown in Figure 7b, the loss curve of GWO-GA-PSO dropped the fastest, falling below 0.1 after 100 iterations. This indicated that the algorithm converged quickly and efficiently found the optimal solution. SA-2DCNN and IFA-XGBoost showed average performance, with final loss values of 0.12 and 0.15, respectively. In summary, GWO-GA-PSO significantly outperformed the other algorithms with fast convergence, high accuracy, and strong stability. To further illustrate its fault discrimination capability, the four algorithms were tested for classification across different datasets. The comparison is shown in Figure 8.

As shown in Figure 8a, the Receiver Operating Characteristic (ROC) Curve of GWO-GA-PSO in the C-MAPSS dataset was close to the upper left corner, with an Area Under the Curve (AUC) of 0.98. Its performance slightly decreased on AeBAD but remained highly generalizable. As shown in Figure 8c, SA-2DCNN performed better than the remaining two algorithms but still worse than GWO-GA-PSO. RVM-ANFIS and IFA-XGBoost showed lower and flatter curves, indicating weaker discrimination ability. Overall, GWO-GA-PSO achieved superior performance on both simulated and real blade datasets, demonstrating the strongest ability to distinguish between fault and normal samples. In order to verify the necessity of each component in the GWO-GA-PSO algorithm, this study conducted an ablation experiment, and the results are shown in Table 3.

From Table 3, it can be seen that the convergence iteration of PSO is 350 times, the proportion of fault sensitive features is 68.2%,

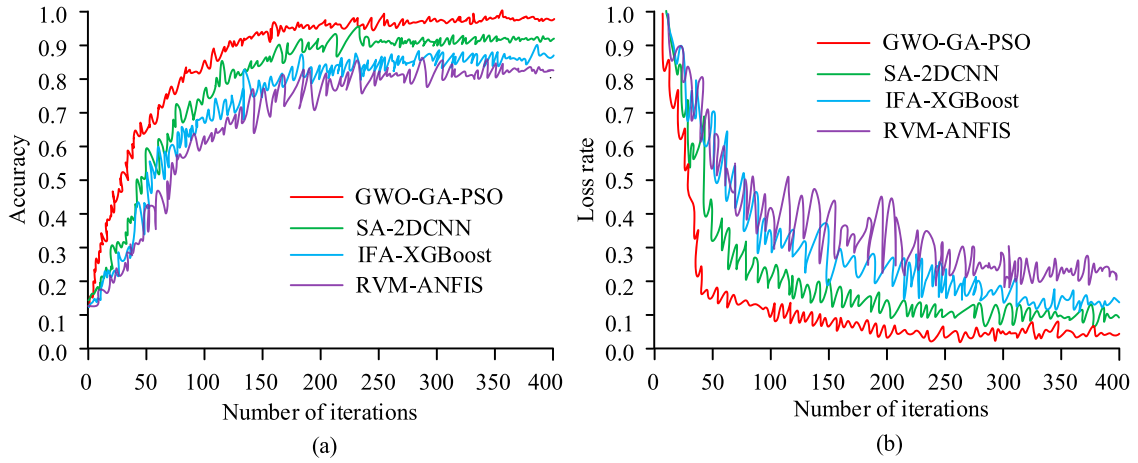

FIGURE 7
Comparison of accuracy and loss rate curves. **(a)** Accuracy curves for the four algorithms. **(b)** Loss rate curves for the four algorithms.

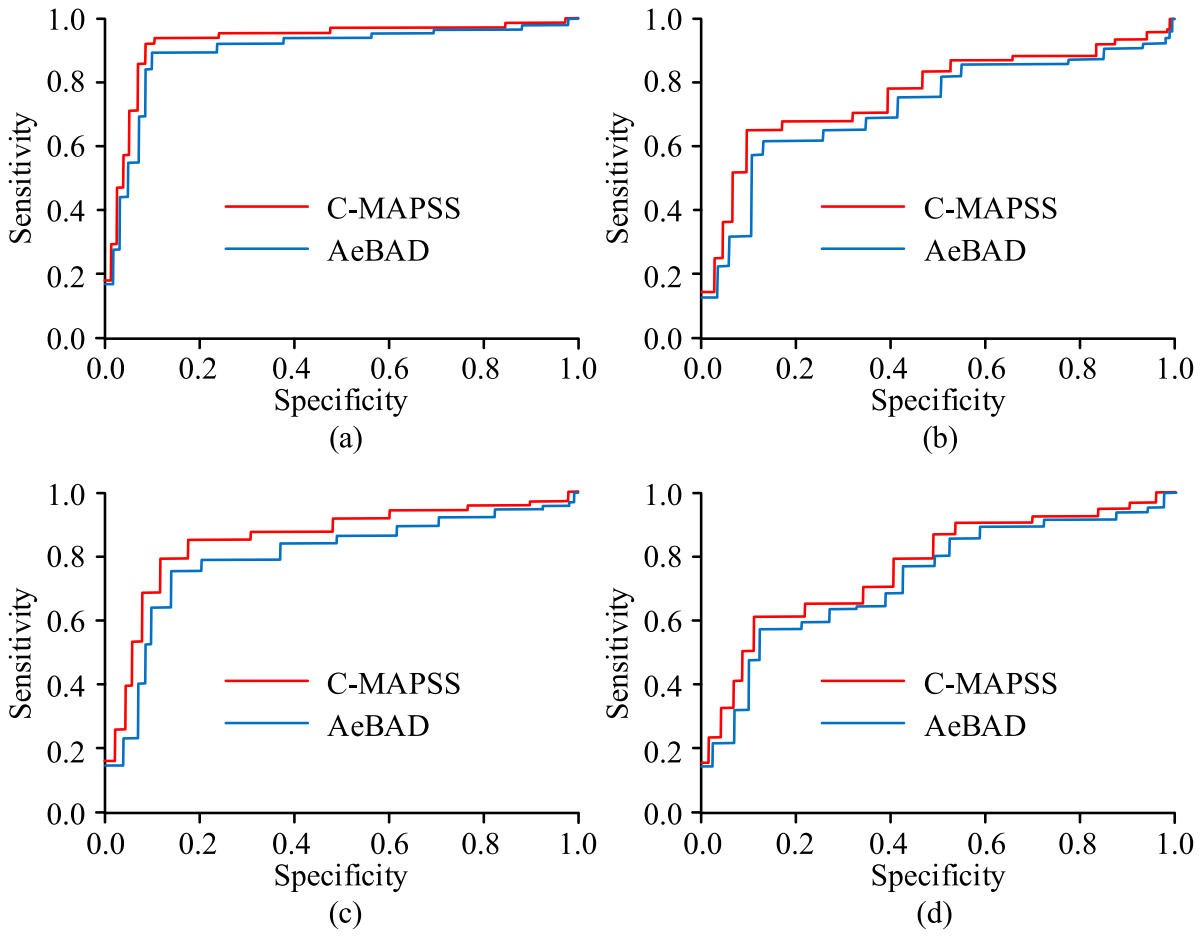

FIGURE 8
Comparison of classification test results in different datasets. **(a)** ROC curves of GWO-GA-PSO in different datasets. **(b)** ROC curves of RVM-ANFIS in different datasets. **(c)** ROC curves of SA-2DCNN in different datasets. **(d)** ROC curves of IFA-XGBoost in different datasets.

and the F1 score is 86.5%. The convergence iteration number of GA-PSO is 240 times, the proportion of fault sensitive features is 80.5%, and the F1 score is 91.2%. Compared to PSO, GA-PSO reduces the number of convergence iterations by 31.4%, increases the proportion of fault sensitive features by 18.0%, and increases F1 score by 4.7%. This indicates that the addition of GA can

TABLE 3 Ablation experiment results.

Algorithm	Convergence iteration times (times)	Proportion of fault sensitive features (%)	F1-score (%)
PSO	350	68.2	86.5
GA-PSO (ablation GWO)	240	80.5	91.2
GWO-PSO (ablation GA)	200	84.3	93.1
GWO-GA-PSO	140	92.7	96.8

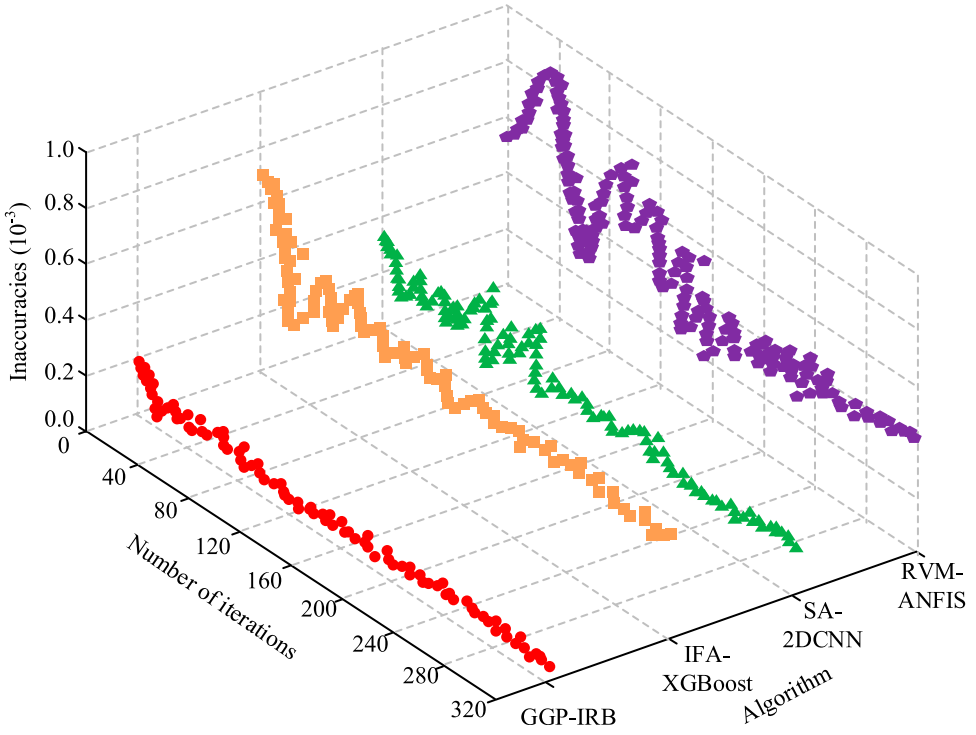

FIGURE 9
Comparison of learning ability and convergence performance.

effectively solve the problem of population homogenization in PSO, avoiding the algorithm from falling into local optima in the later stage of feature selection, and thus filtering out more discriminative fault features. The convergence iteration times, proportion of fault sensitive features, and F1 score of GWO-PSO are 200 times, 84.3%, and 93.1%, respectively. Compared with PSO, the convergence iteration times are reduced by 42.9%, the proportion of fault sensitive features is increased by 23.6%, and the F1 score is increased by 6.6%. The introduction of GWO can accurately focus on the region where the optimal feature subset is located, improving local optimization accuracy. The three indicators of GWO-GA-PSO are 140 times, 92.7%, and 96.8%, respectively, which are significantly better than other sub modules. This indicates that the advantages of GA and GWO can be combined with the global search advantage of PSO, avoiding the disadvantage of single PSO easily falling into local optima, and compensating for the problem of insufficient local search accuracy when GA is optimized alone and limited global exploration range when GWO is optimized alone. The collaboration of the three can more efficiently screen the key sensitive features of turbine blade faults, greatly improve the discrimination of feature subsets, and provide high-quality input for subsequent fault detection models.

4.2 Application evaluation of proposed aircraft engine turbine blade fault detection system

After verifying the performance of GWO-GA-PSO, the GGP-IRB fault detection system based on this algorithm was further evaluated. It was compared with fault detection systems based on SA-2DCNN, RVM-ANFIS, and IFA-XGBoost under the same environment and datasets. The learning ability and convergence performance were compared, as shown in Figure 9.

In Figure 9, the RVM-ANFIS system had the highest loss rate and the slowest decrease, stabilizing after 240 iterations with an error of 0.40×10^{-3}. The SA-2DCNN system decreased more slowly, with a final error of 0.2×10^{-3}. The GGP-IRB system converged the

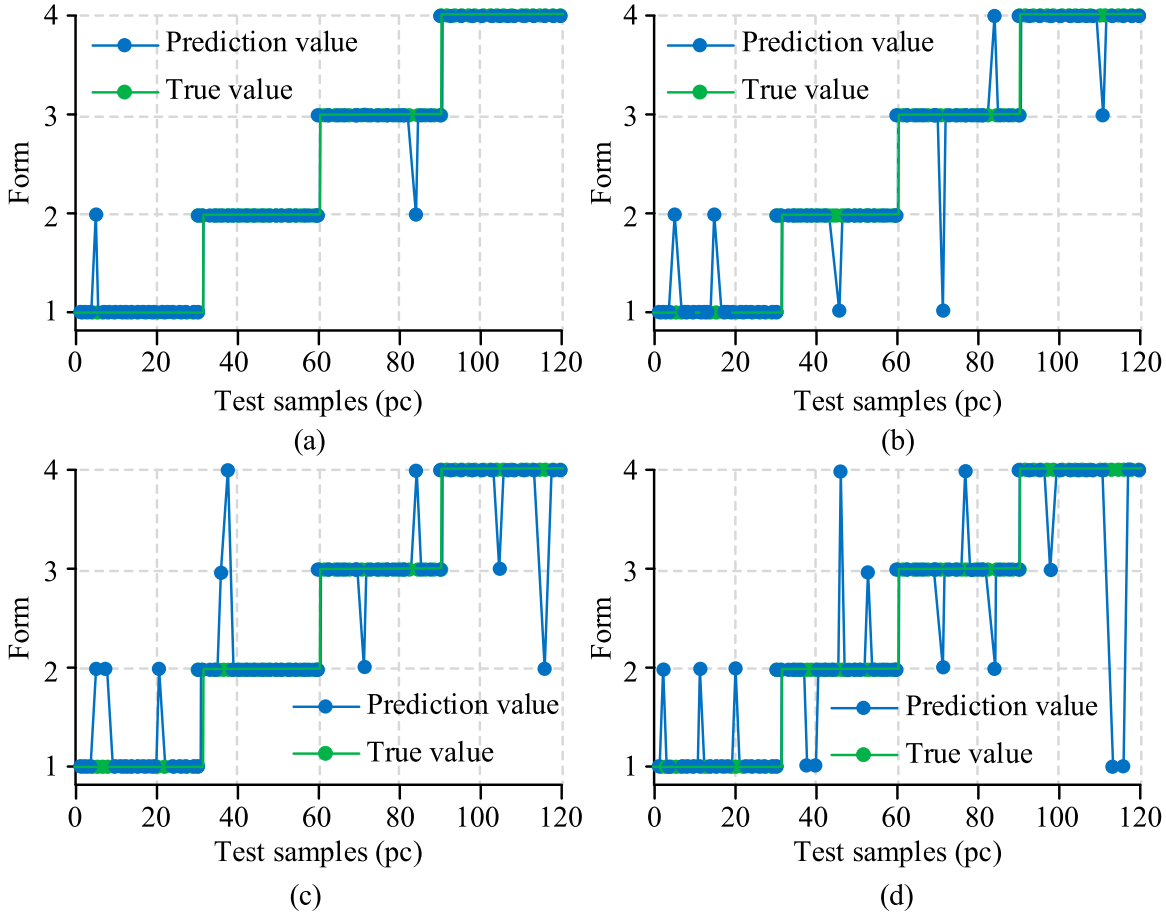

FIGURE 10
Comparison between predicted results and true values. **(a)** GGP-IRB diagnostic results. **(b)** SA-2DCNN diagnostic results. **(c)** IFA-XGBoost diagnostic results. **(d)** RVM-ANFIS diagnostic results.

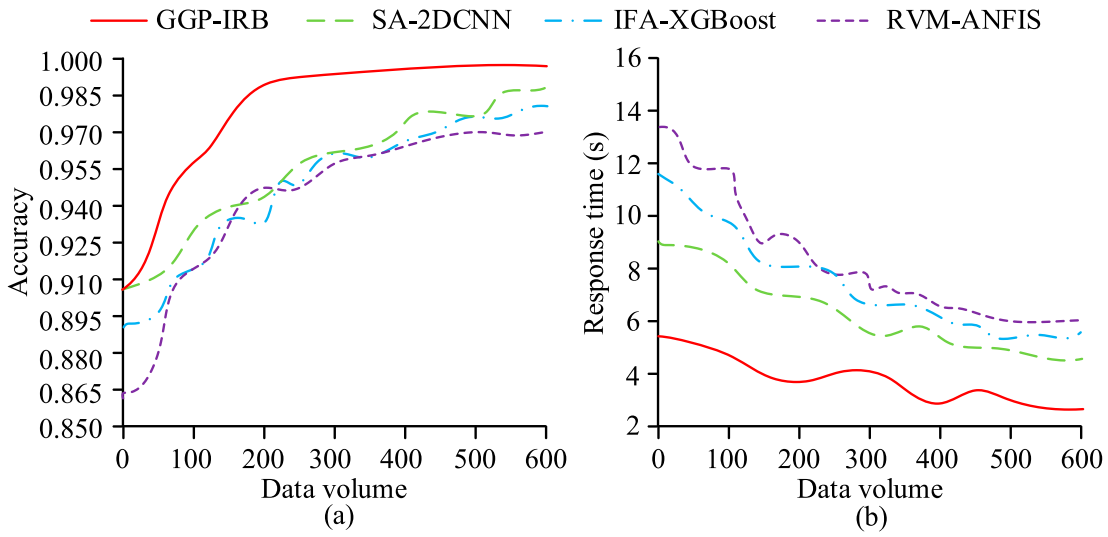

FIGURE 11
Comparison of accuracy and response time results. **(a)** Accuracy curves for the four systems. **(b)** Response time curves for the four systems.

fastest, stabilizing after 80 iterations with an error of 0.08×10^{-3}. Overall, GGP-IRB exhibited the best learning efficiency and convergence performance, significantly outperforming the other systems, making it the optimal choice for aero-engine blade fault detection. To verify its fault detection performance, the four systems were tested on the AeBAD dataset for fault prediction, as shown in Figure 10.

As shown in Figure 10a, the predictions of GGP-IRB were almost identical to the true values, with only two samples showing deviation. Its prediction accuracy reached 98.33%, which was 9.16% higher than RVM-ANFIS at 89.17%, indicating very high precision and stability. As shown in Figure 10b, SA-2DCNN showed some dispersion with an accuracy of 95.00%, but it still outperformed IFA-XGBoost and RVM-ANFIS, suggesting that while it detected faults reasonably well, it was prone to errors on complex noisy samples. As shown in Figures 10c,d, IFA-XGBoost and RVM-ANFIS exhibited severe dispersion, indicating average prediction accuracy and stability. In summary, GGP-IRB achieved the highest prediction accuracy of 98.33% among all systems, showing precise fault state recognition. To further evaluate its performance, the four systems were compared with increasing data volume in terms of accuracy and response time, as shown in Figure 11.

As shown in Figure 11a, as the data volume increased, the accuracy of all four systems improved. GGP-IRB rose sharply when the data volume ranged from 0–200, indicating strong learning ability, and finally reached an accuracy of 0.990. The other systems increased more slowly, with final accuracies of 0.980, 0.972, and 0.965, respectively. As shown in Figure 11b, the response time of GGP-IRB remained the lowest and finally reached 2.5 s as the data volume increased, indicating high computational efficiency. The SA-2DCNN system was slightly slower, with response time decreasing from 9.0 s to 4.9 s. In summary, GGP-IRB significantly outperformed the other systems in accuracy, data efficiency, and real-time capability, effectively detecting aero-engine turbine blade faults.

5 Conclusions and recommendations

This paper addressed the limitations of timeliness and interpretability in traditional turbine blade fault detection systems and aimed to solve the challenge of fault detection in aircraft engine turbine blades to ensure flight safety. An innovative GGP-IRB system was constructed, integrating an improved PSO and an improved RVM to achieve high-precision fault identification. Experimental results showed that the GGP-IRB system exhibited excellent performance on both simulated and real datasets. The GWO-GA-PSO algorithm achieved an accuracy of 98.00% and an AUC of 0.98. After 80 iterations, the minimum error reached 0.08×10^{-3}, and the fault prediction accuracy was 98.33%, which was 9.16% higher than the comparison system. The final response time was only 2.5 s, and the accuracy fluctuated little with changes in data volume, demonstrating strong robustness. Overall, the GGP-IRB system empowered by the improved particle swarm algorithm efficiently and accurately identified turbine blade faults and compensated for the shortcomings of traditional methods. However, this study still had limitations. The system's ability to recognize new faults under extremely complex operating conditions required further improvement, and its long-term stability under large-scale data scenarios was not fully validated. In the future, the system will be optimized to enhance its generalization capability and expand its application scope, providing more reliable support for intelligent maintenance of aircraft engines.

Data availability statement

The original contributions presented in the study are included in the article/supplementary material, further inquiries can be directed to the corresponding author.

Author contributions

JS: Conceptualization, Data curation, Methodology, Writing – original draft, Writing – review and editing.

Funding

The authors declare that financial support was received for the research and/or publication of this article. The research is supported by the Mechanical Arm System for Internal Inspection of Aviation Engines (No.: JATC23010107).

Conflict of interest

The authors declare that the research was conducted in the absence of any commercial or financial relationships that could be construed as a potential conflict of interest.

Generative AI statement

The authors declare that no Generative AI was used in the creation of this manuscript.

Any alternative text (alt text) provided alongside figures in this article has been generated by Frontiers with the support of artificial intelligence and reasonable efforts have been made to ensure accuracy, including review by the authors wherever possible. If you identify any issues, please contact us.

Publisher's note

References

Amjad, M. H. H., Chowdhury, B. R., Reza, S. A., Shovon, M. S. S., Karmakar, M., Islam, M. R., et al. (2025). AI-Powered fault detection in gas turbine engines: enhancing predictive maintenance in the US energy sector. *J. Ecohumanism* 4 (4), 658–678. doi:10.62754/joe.v4i4.6773

An, N., Wang, G., Wang, D., Ma, G., Chang, X., and Zhou, M. (2025). DEM parameter calibration based on multi-objective Bayesian optimization and prior physical information. *Acta Geotech.* 20 (3), 1379–1401. doi:10.1007/s11440-025-02537-7

Bhandari, A. S., Kumar, A., and Ram, M. (2023a). Grey wolf optimizer and hybrid PSO-GWO for reliability optimization and redundancy allocation problem. *Qual. Reliab. Eng. Int.* 39 (3), 905–921. doi:10.1002/qre.3265

Bhandari, A. S., Kumar, A., and Ram, M. (2023b). Reliability optimization and redundancy allocation for fire extinguisher drone using hybrid PSO–GWO. *Soft Comput.* 27 (20), 14819–14833. doi:10.1007/s00500-023-08560-8

Bhandari, A. S., Kumar, A., and Ram, M. (2024). Hybrid PSO-GWO algorithm for reliability redundancy allocation problem with cold standby strategy. *Qual. Reliab. Eng. Int.* 40 (1), 115–130. doi:10.1002/qre.3243

Cuong-Le, T., Nghia-Nguyen, T., Khatir, S., Trong-Nguyen, P., Mirjalili, S. D., and Nguyen, K. (2022). An efficient approach for damage identification based on improved machine learning using PSO-SVM. *Eng. Comput.* 38 (4), 3069–3084. doi:10.1007/s00366-021-01299-6

Demir, S., and Sahin, E. K. (2023). Predicting occurrence of liquefaction-induced lateral spreading using gradient boosting algorithms integrated with particle swarm optimization: pso-xgboost, PSO-LightGBM, and PSO-CatBoost. *Acta Geotech.* 18 (6), 3403–3419. doi:10.1007/s11440-022-01777-1

Dong, L., Chen, Z., Hua, R., Hu, S., Fan, C., and Xiao, x. (2023). Research on diagnosis method of centrifugal pump rotor faults based on IPSO-VMD and RVM. *Nucl. Eng. Technol.* 55 (3), 827–838. doi:10.1016/j.net.2022.10.045

El-Shafiey, M. G., Hagag, A., El-Dahshan, E. S. A., and Ismail, M. A. (2022). A hybrid GA and PSO optimized approach for heart-disease prediction based on random forest. *Multimedia Tools Appl.* 81 (13), 18155–18179. doi:10.1007/s11042-022-12425-x

Khatti, J., and Grover, K. S. (2025). Estimation of uniaxial strength of rock: a comparison between bayesian-optimized machine learning models. *Min. Metallurgy and Explor.* 42 (1), 133–154. doi:10.1007/s42461-024-01168-y

Khodsuz, M., and Mashayekhi, V. (2023). Grounding system impedance influence on the surge arrester frequency-dependent model parameters using PSO-GWO algorithm. *COMPEL-The Int. J. Comput. Math. Electr. Electron. Eng.* 42 (6), 1456–1476. doi:10.1108/compel-07-2022-0229

Kiliçarslan, S. (2023). PSO+ GWO: a hybrid particle swarm optimization and grey wolf optimization based algorithm for fine-tuning hyper-parameters of convolutional neural networks for cardiovascular disease detection. *J. Ambient Intell. Humaniz. Comput.* 14 (1), 87–97. doi:10.1007/s12652-022-04433-4

Li, S., and Fan, Z. (2022). Evaluation of urban green space landscape planning scheme based on PSO-BP neural network model. *Alexandria Eng. J.* 61 (9), 7141–7153. doi:10.1016/j.aej.2021.12.057

Liu, Q., Vassiliadis, V. S., Wu, Y., Zhang, J., Cheng, C., and Yuan, Y. (2023). A quality prediction and parameter optimization approach for turbine blade multistage manufacturing. *IEEE/ASME Trans. Mechatronics* 29 (1), 3–15. doi:10.1109/tmech.2023.3260884

Ogaili, A. A., Hamzah, M. N., Jaber, A. A., and Ghane, E. (2024). Application of discrete wavelet transform for condition monitoring and fault detection in wind turbine blades: an experimental study. *Eng. Technol. J.* 42 (1), 1–13. doi:10.30684/etj.2023.142023.1516

Purohit, J., and Dave, R. (2023). Leveraging deep learning techniques to obtain efficacious segmentation results. *Archives Adv. Eng. Sci.* 1 (1), 11–26. doi:10.47852/bonviewaaes32021220

Rao, C., Liu, Y., and Goh, M. (2023). Credit risk assessment mechanism of personal auto loan based on PSO-XGBoost model. *Complex and Intelligent Syst.* 9 (2), 1391–1414. doi:10.1007/s40747-022-00854-y

Wang, W., Su, H., Liu, X., Munir, J., and Wang, J. (2024). A lightweight convolutional neural network for real-time detection of aircraft engine blade damage. *J. Appl. Sci. Eng.* 28 (8), 1759–1768. doi:10.6180/jase.202508_28(8).0013

Wang, J., Guo, Q. Y., Fu, C. L., Dai, G., Xia, C. Y., and Qian, L. Q. (2025). A novel optimization scheme for structure and balance of compound balanced beam pumping units using the PSO, GA, and GWO algorithms. *Petroleum Sci.* 22 (3), 1340–1359. doi:10.1016/j.petsci.2025.01.007

Xu, C., Gui, X., and Zhao, Y. (2024). Digital twin-assisted multiview reconstruction enhanced domain adaptation graph networks for aero-engine gas path fault diagnosis. *IEEE Sensors J.* 24 (13), 21694–21705. doi:10.1109/jsen.2024.3400249